



University of Tennessee, Knoxville

TRACE: Tennessee Research and Creative Exchange

Masters Theses

Graduate School

12-1998

Vorticity confinement application to flow around circular cylinders

Lifan Yu

Follow this and additional works at: https://trace.tennessee.edu/utk_gradthes

Recommended Citation

Yu, Lifan, "Vorticity confinement application to flow around circular cylinders. " Master's Thesis, University of Tennessee, 1998.

https://trace.tennessee.edu/utk_gradthes/10430

This Thesis is brought to you for free and open access by the Graduate School at TRACE: Tennessee Research and Creative Exchange. It has been accepted for inclusion in Masters Theses by an authorized administrator of TRACE: Tennessee Research and Creative Exchange. For more information, please contact trace@utk.edu.

To the Graduate Council:

I am submitting herewith a thesis written by Lifan Yu entitled "Vorticity confinement application to flow around circular cylinders." I have examined the final electronic copy of this thesis for form and content and recommend that it be accepted in partial fulfillment of the requirements for the degree of Master of Science, with a major in Mechanical Engineering.

John Steinhoff, Major Professor

We have read this thesis and recommend its acceptance:

John Caruthers, Charles Merkle

Accepted for the Council:

Carolyn R. Hodges

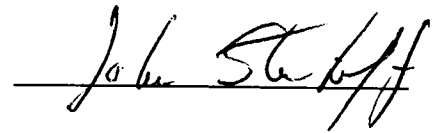
Vice Provost and Dean of the Graduate School

(Original signatures are on file with official student records.)

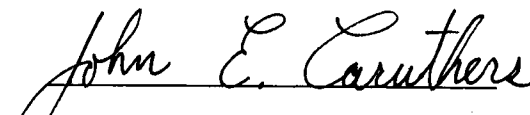
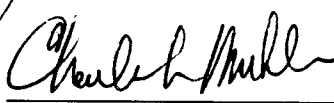
July 24, 1998

To the Graduate Council:

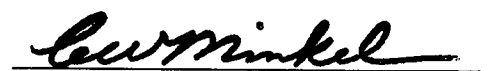
I am submitting herewith a thesis written by Lifan Yu, entitled "Vorticity Confinement Application To Flow Around Circular Cylinders." I recommend that it be accepted in partial fulfillment of the requirements for the Master's Degree, with a major in Mechanical Engineering.


Major Professor

We have read this thesis and
recommend its acceptance:

Accepted for the council:


Vice Chancellor for
Graduate Studies and Research

Vorticity Confinement Application To Flow Around Circular Cylinders

A Thesis
Presented for the
Master of Science Degree
The University of Tennessee, Knoxville

Lifan Yu
December 1998

Acknowledgement

I would like to express my deepest gratitude to my advisor, Dr. John Steinhoff, for his continual assistance, support and technical guidance. I also appreciate all the comments and advice from Dr. John Caruthers, Dr. Charles Merkle, Dr. K.C. Reddy and Dr. Frank Caradonna. Sincere thanks are extended to Ms. Mary Lo and other library personnel for their assistance, and to all my friends who helped me in a variety of ways during my studies.

This work was funded by the Army Research Office and by the University of Tennessee Space Institute.

From the bottom of my heart, I would like to thank my parents and my brother who love, care, and support me all the time.

Abstract

Many flows which CFD is dealing with involve very thin vortical layers including boundary layers and shed vorticity. Conventionally, people have to use very fine grids and high order discretization to try to get the details of the internal structure of these thin vortical regions. Those methods may cost lots of computation time and still cannot give the right solutions. For example, in many of these flows the solutions near the surface can be determined by the details of the shed vorticity as much as by those of the internal structure of the boundary layer. A generalized *Vorticity Confinement* method, developed by John Steinhoff, represents the vortical layers as solitary wave solutions. This method involves adding a nonlinear negative diffusion term to the discretized momentum equations. Instead of the details of the internal structure, the integral effects of the thin region is computed, obeying the mass and momentum conservation laws. In addition to efficiently computing transport of shed vorticity, it allows the use of regular Cartesian coarse grids, which enables us to get reasonable solution without grid generation effort and with much less computation than other methods.

The *Vorticity Confinement* method is applied to compute for flow around circular cylinders. This research is the first step towards the development of boundary layer models for blunt bodies in an incompressible flow. In this first step, only the "bare" scheme is used, without any "tunable" turbulence models.

Contents

1	Introduction	1
1.1	Background	1
1.2	Objectives	4
2	Vorticity Confinement Method For Cartesian Grids	6
2.1	Solitary Wave	7
2.2	Vorticity Confinement	7
2.2.1	How To Create A Solitary-wave-like Solution	7
2.2.2	" F " Function and Cartesian Grids	9
2.2.3	Outline of Method	10
2.2.4	Vorticity And Momentum Conservation	12
2.3	Physical Understanding of Vorticity Confinement Method On Boundaries	14
3	Applications To Flow Around Circular Cylinders	16
3.1	Numerical Procedures	16
3.1.1	" F " function	16
3.1.2	Velocity Convection	17
3.1.3	Vorticity Confinement	19

3.2	Test Cases and Results	22
3.2.1	Case 1: Circular Flow	22
3.2.2	Case 2: Uniform Far Field Flow	32
4	Conclusion	52
	Bibliography	54
	Vita	58

List of Figures

3.1	Diagram of Convection Computation	18
3.2	Staggered Discretization To Compute Vorticity	19
3.3	Flow Boundaries	23
3.4	Initial Flow Velocity Field	24
3.5	Initial Vorticity Contours, $t = 0$; $\omega_{max} = 0.9597$, $\omega_{min} = 0.0639$	25
3.6	Expanded View of Vorticity Contours with <i>Vorticity Confinement</i> , $t =$ 1024; $\omega_{max} = 0.7474$, $\omega_{min} = 0.0639$	26
3.7	Expanded View of Vorticity Contours without <i>Vorticity Confinement</i> , $t = 1024$; $\omega_{max} = 0.6347$, $\omega_{min} = 0.0639$	26
3.8	Initial Vorticity-radius	28
3.9	$\omega - r$ with <i>Vorticity Confinement</i> , $t = 1024$	28
3.10	$\omega - r$ without <i>Vorticity Confinement</i> , $t = 1024$	29
3.11	$q_r - r$ with <i>Vorticity Confinement</i> , $t = 1024$	29
3.12	$q_r - r$ without <i>Vorticity Confinement</i> , $t = 1024$	30
3.13	Initial $q_t - r$	30
3.14	$q_t - r$ with <i>Vorticity Confinement</i> , $t = 1024$	31
3.15	$q_t - r$ without <i>Vorticity Confinement</i> , $t = 1024$	31

3.16	Variation of St in terms of Re , Roshko(1954P)	35
3.17	Compilation of St versus Re : (a) Drescher(1956J) \circ French data, \square Tyler, \diamond DVL data, \bigcirc AVA($Re > 1k$) (b) Etkin <i>et al.</i> (1957J)	36
3.18	Initial Velocity Field	38
3.19	Velocity Field; $t = 1024$	38
3.20	Vorticity Contours; $R_c = 10$; $t = 992$	39
3.21	Vorticity Contours; $R_c = 10$; $t = 1024$	39
3.22	Expanded View of Vorticity Contours; $R_c = 10$; $t = 1024$; $\omega_{max} =$ 1.063 , $\omega_{min} = 0.2$	40
3.23	Expanded View of the Vorticity Contours; $R_c = 10$; $t = 992$	41
3.24	Expanded View of the Vorticity Contours; $R_c = 10$; $t = 1024$	41
3.25	Vorticity Contours with Reduced ε_ω ; $R_c = 10$; $t = 1024$	43
3.26	Vorticity Contours; $R_c = 10$; <i>Grids</i> : 640×128 ; $t = 2048$	43
3.27	Expanded View of Vorticity Contours; $R_c = 5$; $t = 1024$; $\omega_{max} = 1.026$, $\omega_{min} = 0.2$	44
3.28	Vorticity Contours; $R_c = 5$; $t = 1008$	45
3.29	Vorticity Contours; $R_c = 5$; $t = 1024$	45
3.30	Expanded View of Vorticity Contours; $R_c = 5$; $t = 1008$	46
3.31	Expanded View of Vorticity Contours; $R_c = 5$; $t = 1024$	46
3.32	Vorticity Contours; $R_c = 2.5$; $t = 1016$	47
3.33	Vorticity Contours; $R_c = 2.5$; $t = 1024$	47
3.34	Expanded View of Vorticity Contours; $R_c = 2.5$; $t = 1016$	48
3.35	Expanded View of Vorticity Contours; $R_c = 2.5$; $t = 1024$	48

3.36 Expanded View of Vorticity Contours; $R_c = 2.5$; $t = 1024$; $\omega_{max} =$	
1.104, $\omega_{min} = 0.2$	49

Chapter 1

Introduction

1.1 Background

There are many vortex-dominated flows of engineering interest. During the past several decades, people have tried to find reliable numerical methods to solve for these flows. Eulerian methods and Lagrangian methods are the two classes of conventional numerical schemes used[2][5].

In Eulerian methods, body-fitted grids can be used effectively with discretized Navier-Stokes flow equations for flows at low Reynolds numbers where boundary layer as well as shed vorticity is spread over a rather wide region and remains laminar. However, flows at high Reynolds numbers are very different: the boundary layer and the shed vorticity can be very thin and the flow can be turbulent. To treat thin vortical regions, people apply techniques like high-order discretization and adaptive grid schemes using very fine grids. Such schemes require a large amount of computing. As for adaptive grid schemes, although extra grid points are embedded in the vortical regions, they cannot economically capture the shed vortex without having it spread over a region much larger than measured in experiments, especially for time

dependent flows where the grid must be continually adapted. To compute the internal structure of these features accurately over a long time using Euler/Navier-Stokes numerical schemes with very fine grids may not be practicable or even necessary. Further, in most high Reynolds number flows only an approximate (turbulent) model to the Navier-Stokes equation is solved. In these cases the final result is, of course, a reflection of the model instead of the actual Navier-Stokes equations.

In Lagrangian methods, some of the most efficient ones for treating thin vortical flows currently involve Lagrangian marker-based schemes, where vorticity or circulation is assigned to individual markers which convect through the flow field. Unfortunately, since the vortical regions are defined by connected sets of markers, the topology of each region should be known beforehand so that suitable arrays of markers can be computationally defined. In general, the vortical regions may interact with solid surfaces and their topology may change. This requires new specifications of the markers and re-connection. In addition, vortical regions cannot easily be made to merge in a natural way if they are defined by markers. Lagrangian methods which use large numbers of unconnected markers with overlapping structure also appear to require information on the locations of vortical regions for efficient allocation of markers.

The fact behind the Lagrangian marker-based schemes is that the internal structure of vortical regions is often not important since the dimension of these structures is small compared to other dimensions of the problem. As long as the centroid of these vortices and the total circulation surrounding the vortices are computed accurately, the overall solution will often be accurate. That is the beginning thought of the

new method – *Vorticity Confinement*. Further, this method is intended to be a very efficient "zeroth order" starting point, from which perturbation terms can be added to treat phenomena that depend on the internal details of the structures.

This approach is similar to the treatment of shock waves in conventional numerical methods, which are "captured" over a small number of regular grid cells, rather than accurately solved by a viscous computation. Since the physical shock thickness is typically much smaller than the other dimensions of the problem, as long as they are captured over a small region and conservation laws are obeyed in integrated form, the numerical solution of the overall flow field can be accurate for most practical purposes: i.e., where accurate solution of the internal structure is not necessary. Then the computational grid and time step size can be determined by the overall problem instead of the thin structure.

We would like to treat very thin physical vortical layers in a similar way. In a shock wave, the characteristics slope into the shock centroid, helping to capture it over very few grid cells. Vortical phenomena do not have this feature and are more difficult to capture using conventional methods.

Without using fine grids, structures similar to so-called solitary waves are applied in the *Vorticity Confinement* method[3][4][6]. These solitary waves can propagate over arbitrary distances with fixed, thin shape on a uniform Cartesian lattice of grid points. Their structure is an exact result of the numerical scheme rather than the result of an approximate discretization of a viscous term in a partial differential equation.

A smooth interpolation function " F " is used to represent the configuration of the body where the surface is a "level set" of this function. By adding a *Vorticity*

Confinement term based on " F " to the discretized momentum equations, we can convect the boundary layer-like solitary wave layers without diffusion. Then, only a regular Cartesian grid is needed with no requirement for a body-conforming grid. In this way, we can get reasonable solutions much more easily and efficiently than with conventional methods.

1.2 Objectives

There are two parts which are very important in the computation of blunt bodies in a high Reynolds number flow - the free wake and the surface boundary layer.

Usually, the flow has some features like turbulence and thin vortical regions. In both cases, there are no equations that can be solved exactly on current computers. People can only try to model to get an approximation. We want to develop a way to implement models (if necessary) efficiently without using fine grids, or just to capture the shed vortice with our current method if details of the internal structure are not important.

In addition, for surface boundary layers, we also want to get separations at the right times and places, which is most important for blunt bodies.

Since we prefer to use regular non-body-conforming Cartesian grids, the computed flow in the boundary will not be more accurate than that of near free wake; the same treatment will be used for the boundary surface and free wake. This leads to a consistent treatment of free and bound vorticity. To have a more accurate fine grid body conforming surface discretization does not seem to increase the overall solution accuracy for these flows because strong shed vorticity is often close by, which also

must be computed.

This research is meant to demonstrate that the initial "bare" *Vorticity Confinement* method with no modeling terms can approximately satisfy the above requirements, by studying a problem that has all of the important flow features for blunt body incompressible flow: boundary layers can be turbulent and large amounts of vorticity can be shed in a highly unsteady way, and the shed vorticity in turn influences the flow near the boundary. Also, this shed vorticity ultimately becomes turbulent and must be modeled (a subject for future study).

The particular problem chosen, the circular cylinder, has a very rich variety of boundary layer/wake behaviors depending on Reynolds numbers and has not yet been accurately treated at high Reynolds numbers even though it has been studied by a large number of researchers over many years. Thus, it seems to be an ideal testing ground both for this initial study of the "bare" method and for further development of special turbulence models within the *Vorticity Confinement* approach.

Chapter 2

Vorticity Confinement Method For Cartesian Grids

Conventionally, people use equations with modeled dissipative terms, which resemble Navier-Stokes equations, to approximate high Reynolds number turbulent flow problems. When discretizing the basic equations, there is usually significant numerical diffusion. Unless very fine grids are used, this numerical diffusion can be much greater than the modeled turbulent diffusion, especially in the boundary layers. *Vorticity Confinement* is a method to create solitary-wave-like configurations of concentrated vorticity which have a thickness of only 2-3 grid cells. They are created by adding a simple term to the discretized momentum conservation equations[3][4] for incompressible flow. The added term is used together with a numerical diffusion(which may be large on coarse grids) to create a model for the structure in a very efficient way. The terms are based on a continuum form that is inherently multidimensional and rotationally invariant, depending only on local variables and vanishing outside the vortical regions. So, simple low-order diffusive numerical schemes can be used to discretize and solve the modified flow equations on relatively coarse grids, without

resulting in vortices that spread as they convect.

This method involves a regular Eulerian Cartesian computational grid and a smooth " F " function defined on the grid which implicitly defines the body surface as a "level set".

The method combines the advantages of both Eulerian and Lagrangian methods. It uses regular Cartesian non-body-conforming grids. Further, it allows the general interaction of vortical regions, which is a characteristic of Eulerian methods. Its ability to resolve the vortical regions precisely is as good as Lagrangian ones[3][5].

2.1 Solitary Wave

The solitary wave, so called because it often occurs as a single localized entity, was first observed by J.Scott Russell in 1834. It can travel over a long distance without changing its shape. In high Reynolds number incompressible flow, this is true for most thin vortical layers too. In the *Vorticity Confinement* method, by adding a nonlinear negative viscosity term to the discretized Navier-Stokes equations, we can get solitary-wave-like solutions spread over 2-3 grid cells.

Here, the solitary wave is not meant to approximate the internal structure of the actual thin feature or layer. Instead, it is meant to represent the layer as, for example, an interpolating function.

2.2 Vorticity Confinement

2.2.1 How To Create A Solitary-wave-like Solution

The basic idea of the *Vorticity Confinement* method is to create "thin" regions in the computational grid, where vorticity is large. These regions represent boundary

layers on solid surfaces or separated, convecting vortex sheets or filaments. It is expected that many of the actual physical vortical regions in high Reynolds number flows are thinner than a grid cell (for example, a tip vortex from a wing). By adding a non-linear "negative viscosity" term in the discretized momentum equations, we can get solitary-wave-like solutions that behave like these vortices, i.e.- have the correct velocity outside a numerical "core" and have correct motion of the centroid. For layers representing boundary layers, similar considerations can be applied.

In the following, we describe the simple "bare" *Vorticity Confinement* method which gives reasonable approximate results for a large number of problems. Based on this, more careful modeling terms are to be added in future studies to refine the results, especially for high Reynolds number flows. We model the diffusive effects of the numerical method with a diffusion term in the momentum equation and look at the results of this method. For 3-D unsteady incompressible flows, the governing equation with the confinement term and the diffusive model of the numerical method are:

$$\nabla \cdot \vec{q} = 0 \quad (2.1)$$

$$\partial_t \vec{q} = -(\vec{q} \cdot \nabla) \vec{q} - \nabla \left(\frac{p}{\rho} \right) + \mu \nabla^2 \vec{q} + \varepsilon \vec{s} \quad (2.2)$$

where \vec{q} is the velocity vector, p pressure, and ρ density. (2.2) is the momentum equation with two additional terms added on the right. The third term on the right of (2.2) is the diffusion term, and μ is an effective diffusion parameter. The fourth term on the right of (2.2) is the confinement term. ε is a numerical parameter which, together with μ , controls the size of the convecting vortical regions. The confinement

term has the form

$$\vec{s} = -\hat{n} \times \vec{\omega} \quad (2.3)$$

$$\hat{n} = \frac{\nabla \eta}{|\nabla \eta|} \quad (2.4)$$

$$\vec{\omega} = \nabla \times \vec{q} \quad (2.5)$$

where $\vec{\omega}$ is the vorticity vector and η is a scalar field that has a local minimum on the centroid of the vortical region. For convecting vorticity,

$$\eta = -|\vec{\omega}| \quad (2.6)$$

and for bound vorticity

$$\eta = |F| \quad (2.7)$$

where F is a scalar field, described in the next section.

In the confinement term, \hat{n} is a unit vector pointing away from the centroid of the vortical region, \vec{s} acts as an acceleration in the tangential direction, and the confinement term serves to convect vorticity back towards the centroid as it diffuses away. This convection increases the diffusion term and a steady state distribution results when the two terms become balanced.

2.2.2 "F" Function and Cartesian Grids

For free convecting vortices, the vorticity itself is used in the nonlinear terms required to define the solitary wave. For a solid surface with a boundary layer, a separate smooth "F" function is used to specify the surface as a "level set". The gradient of this function is used in the nonlinear term to create the surface layer as described in the above section. The interpolation function "F" can be used to locate

the layer and should remain locally fixed in shape about the layer. With the Cartesian grid technique, the " F " function is first generated from a given body geometry such that it is zero on the body points, positive outside and negative inside. The value of this function, $F(\vec{x})$, at a grid point is taken to be the (signed) distance from the grid point to the defined surface. Thus, the "level set" values of \vec{x} such that $F(\vec{x}) = 0$ implicitly defines the surface over which the flow is to be solved. This $F = 0$ surface can be complicated and even move according to dynamical equations.

Based on F , a function $\lambda(F)$ is defined, for example, as:

$$\lambda(F) = \begin{cases} 0, & F \leq 0 \\ 1, & F > 0 \end{cases}$$

So we can use $\lambda(F)$ to differentiate the body from the flow, and treat the whole field in the same way without using any conforming grids.

2.2.3 Outline of Method

An outline of *Vorticity Confinement* method is as follows:

1. First, the F function is defined. Then the velocity, \vec{q}^n , is multiplied by $\lambda(F)$, which is the "level set" discribed in the above section.

$$\vec{q}^l = \lambda(F)\vec{q}^n \quad (2.8)$$

This step enforces no-flow-through and no-slip boundary conditions.

2. A convection-like computation is made to treat part of the momentum equation, as in conventional incompressible "split velocity" methods. This is a space-discretized version of

$$\vec{q}^{l'} = \vec{q}^l - \Delta t \vec{q}^l \cdot \nabla \vec{q}^l \quad (2.9)$$

This step approximates the first term on the right hand side of equation (2.2).

3. *Vorticity Confinement*, is used to compute a velocity increment such that a thin vortical structure is obtained even though step 2 has large numerical diffusion (because the grid cells are not thin):

$$\vec{q}''' = \vec{q}'' + \varepsilon \Delta t \hat{n} \times \vec{\omega} + \mu \Delta t \nabla^2 \vec{q}'' \quad (2.10)$$

where $\vec{\omega}$ is vorticity, ε could be ε_s and ε_w which are confinement parameters for solid surface and free vortex, respectively. And \hat{n} could be

$$\hat{n}_s = \frac{\nabla |F|}{|\nabla |F||} \quad (2.11)$$

$$\hat{n}_w = -\frac{\nabla |\omega|}{|\nabla |\omega||} \quad (2.12)$$

for solid surface and free vortex, respectively. μ is the diffusion parameter, μ_w and μ_s , for solid surface and free vortex, respectively. This is a crucial step: it advects vorticity back towards the $F = 0$ surface and centroids of convecting vortical regions. Since only large regular Cartesian grid cells are used, rather than very thin body-fitted cells as in conventional viscous computation, vorticity would continually diffuse away without this step. Then this would lead to a highly viscous low Reynolds number solution which is unwanted.

This step includes the last two terms of the modified momentum equation (2.2).

4. The velocity at the next time step is computed,

$$\vec{q}^{n+1} = \vec{q}''' + \nabla \phi \quad (2.13)$$

where

$$\nabla^2 \phi = -\nabla \cdot \vec{q}''' \quad (2.14)$$

This involves solving a Poisson equation to get ϕ . ϕ is from the second term in the equation (2.2),

$$\phi = -\Delta t p / \rho \quad (2.15)$$

Putting (2.13) into (2.14) results in

$$\nabla \cdot \vec{q}^{n+1} = 0 \quad (2.16)$$

which is the continuity equation. We call this step "Mass Balance".

This step enforces equation (2.1).

2.2.4 Vorticity And Momentum Conservation

An important feature of the *Vorticity Confinement* method is that the correction as well as the diffusion is limited to the vortical regions. Outside the vortical region, $\vec{\omega} = 0$ and the vorticity confinement term in (2.2), $\varepsilon \hat{n} \times \vec{\omega}$, vanishes. In addition,

$$\begin{aligned} \nabla \times \vec{\omega} &= \nabla \times (\nabla \times \vec{q}) \\ &= \nabla(\nabla \cdot \vec{q}) - \nabla \cdot (\nabla \vec{q}) \end{aligned} \quad (2.17)$$

Since for incompressible flows, $\nabla \cdot \vec{q} = 0$,

$$\nabla^2 \vec{q} = -\nabla \times \vec{\omega} \quad (2.18)$$

So, the diffusion term $\mu \nabla^2 \vec{q}$ vanishes too.

Another important feature concerns the total change induced by the correction in vorticity (δI_ω), integrated over the vortical regions. In general 3-D flow, the vorticity

change is zero since $\vec{\omega}$ vanishes outside the vortical regions.

$$\begin{aligned}
\delta I_\omega &= \int_V (\nabla \times \delta \vec{q}) dv \\
&= \int_V \nabla \times (\mu \nabla^2 \vec{q} + \varepsilon \vec{s}) dv \\
&= \mu \int_V \nabla \times (\nabla \times \vec{\omega}) dv + \varepsilon \int_V \nabla \times (-\hat{n} \times \vec{\omega}) dv \\
&= -\mu \int_A (\nabla \times \vec{\omega}) \times d\vec{a} + \varepsilon \int_A (\hat{n} \times \vec{\omega}) \times d\vec{a} \\
&= 0
\end{aligned} \tag{2.19}$$

where $\delta \vec{q} = \mu \nabla^2 \vec{q} + \varepsilon \vec{s}$ is the correction added in equation (2.10).

Another important quantity that is almost conserved with the method is momentum. Here we have a more limited argument. If we have a thin vortical "tube" that is slowly varying along its length, then we can take a 2-D section and write for the change in momentum there:

$$\begin{aligned}
\delta I_p &= \rho \int_A \delta \vec{q} da \\
&= \rho \int_A (\varepsilon \vec{s} + \mu \nabla^2 \vec{q}) da
\end{aligned} \tag{2.20}$$

where the integral is over the 2-D section. In general, δI_p will not be zero. However, for the class of convecting $\vec{\omega}$ distributions that result in our axisymmetric computations, δI_p will vanish.

$$\varepsilon \vec{s} + \mu \nabla^2 \vec{q} = f(r) \hat{e}_\theta \tag{2.21}$$

$$\delta I_p = \rho \int f(r) r dr \int_0^{2\pi} \hat{e}_\theta d\theta = 0 \tag{2.22}$$

A small correction can easily be implemented to make the method exactly conserve momentum; but this correction would be insignificant for the actual flows that we

have considered to date. For boundary layer flows, the net added momentum is cancelled by that transferred to the wall.

2.3 Physical Understanding of Vorticity Confinement Method On Boundaries

Basically, *Vorticity Confinement* itself can be thought of as a crude boundary layer model, when applied to a numerical boundary layer computations. The following is a very heuristic discussion of the physics.

The method creates concentrated vortical regions with zero normal velocity about a surface defined by the zero values of a smooth function $F(\vec{x})$ and thereby simulates physical boundary layers. Every time step, an acceleration is applied to the boundary layer in the tangential direction so that the vortical regions are squeezed. When this effect balances the diffusion effect, a steady state results (actually "quasisteady", since the layer can convect along the surface and change its tangential momentum).

The method also simulates viscous momentum loss in the layers so that they approximate the dynamics of a physical viscous boundary layer. Since the momentum equations resemble Burger's equation in the tangential direction, with a forcing function for the tangential velocity, as in shock waves formation, large tangential velocity gradients may occur. According to mass conservation, large tangential velocity gradients will lead to large normal velocity gradients. This overcomes the confinement term and vorticity can erupt from the surface at this point, leading to smooth surface separation. This separating vorticity is then automatically captured by the vorticity confinement method. Further, the confinement induced tangential acceleration acts

like that in an actual turbulent layer so that this separation does not occur immediately, as it would in a laminar physical layer in an adverse pressure gradient, but is delayed.

Chapter 3

Applications To Flow Around Circular Cylinders

In this chapter, the *Vorticity Confinement* method is applied to investigate flow around circular cylinder cases. One is a circular flow around the cylinder, the other is a uniform far field flow. The numerical procedures will be described first. Then for different cases, results and discussions will be given.

3.1 Numerical Procedures

3.1.1 "F" function

Although the cylinder configuration is very simple to represent, to be consistent with the general method, a scalar function "F" is introduced. "F" is defined at each grid node:

$$F_{i,j} = r_{i,j} - R_c \quad (3.1)$$

where

$$r_{i,j} = \sqrt{(x_{i,j} - x_c)^2 + (y_{i,j} - y_c)^2}$$

and x_c and y_c are the coordinates of the cylinder center, R_c is the radius of the cylinder. Then " $\lambda(F)$ " is defined as

$$\lambda(F_{i,j}) = \begin{cases} 0, & F_{i,j} \leq 0, \\ 1, & F_{i,j} > 0. \end{cases}$$

$$\vec{q}'_{i,j} = \lambda(F_{i,j}) \vec{q}^n_{i,j} \quad (3.2)$$

where $\vec{q} = (u, v)^\dagger$ in this 2-D problem, u and v are velocity components in x and y direction, respectively, at node (i, j) and the current time level n .

3.1.2 Velocity Convection

The velocity field at the next time level $n + 1$ at node (i, j) can be interpolated from the current velocity field. The flow particle which will arrive at node (i, j) at time step $n + 1$, is at point A at time step n in Figure 3.1. Assume Δt is small enough so that A is in one of the neighbouring cells of node (i, j) . A horizontal line and a vertical one are defined to split the cell into four quad areas s_1, s_2, s_3, s_4 , as in Figure 3.1. This is a type of first order upwind explicit scheme. It is unconditionally stable but very diffusive.

$$\vec{q}''_{i,j} = s_1 \vec{q}'_{i,j-1} + s_2 \vec{q}'_{i-1,j-1} + s_3 \vec{q}'_{i,j} + s_4 \vec{q}'_{i-1,j} \quad (3.3)$$

where

$$\begin{aligned} s_1 &= (1 - \nu_x) \nu_y \\ s_2 &= \nu_x \nu_y \\ s_3 &= (1 - \nu_x)(1 - \nu_y) \\ s_4 &= \nu_x(1 - \nu_y) \end{aligned}$$

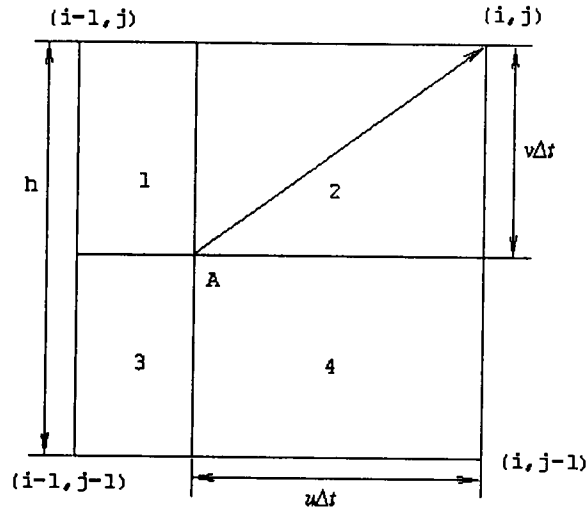


Figure 3.1: Diagram of Convection Computation

$$\nu_x = u\Delta t/h$$

$$\nu_y = v\Delta t/h$$

and h is the cell size. As explained in Chapter 2, the thin vortical region is treated as a thin pulse. By using the above first order upwind finite difference method to convect this thin pulse, a non-isotropic second order numerical diffusion is introduced. The centroid of the pulse may shift by the correct amount, but its shape may change. So we subtract the leading part of this non-isotropic diffusion and add an isotropic diffusion for stability. Noticing that when

$$\nu_x = \nu_y = \frac{1}{2}$$

$$\frac{\nu_x(1 - \nu_x)}{2} = \frac{\nu_y(1 - \nu_y)}{2} = \frac{1}{8}$$

we apply the following fomula:

$$\vec{q}_{i,j}''' = \vec{q}_{i,j}'' + \left(\frac{1}{8} - \frac{\nu_x(1-\nu_x)}{2}\right)\delta_i^2 \vec{q}_{i,j}'' + \left(\frac{1}{8} - \frac{\nu_y(1-\nu_y)}{2}\right)\delta_j^2 \vec{q}_{i,j}'' \quad (3.4)$$

where δ_i^2 and δ_j^2 are central differences in the x and y directions, respectively:

$$\delta_i^2 \vec{q}_{i,j} = \frac{\vec{q}_{i+1,j} - 2\vec{q}_{i,j} + \vec{q}_{i-1,j}}{2h}$$

$$\delta_j^2 \vec{q}_{i,j} = \frac{\vec{q}_{i,j+1} - 2\vec{q}_{i,j} + \vec{q}_{i,j-1}}{2h}$$

3.1.3 Vorticity Confinement

Vorticity Computation

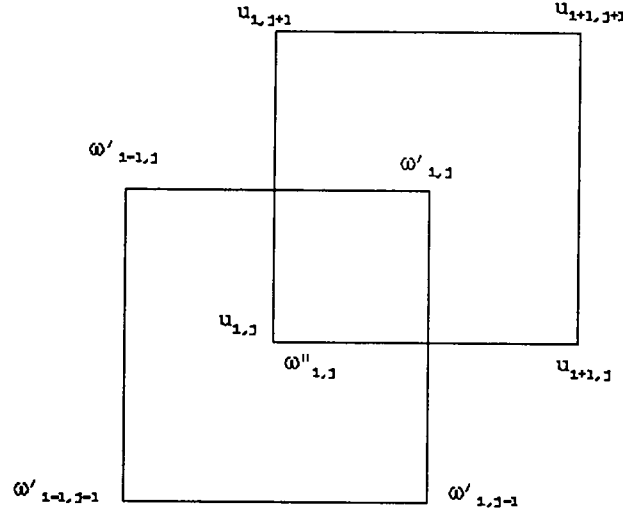


Figure 3.2: Staggered Discretization To Compute Vorticity

First, the vorticity field is computed at each cell center (see Figure 3.2):

$$\vec{\omega} = \nabla \times \vec{q} \quad (3.5)$$

Then, the result is only a single vorticity component in the out of plane direction:

$$\omega = \frac{\partial v}{\partial x} - \frac{\partial u}{\partial y} \quad (3.6)$$

Numerically, we can get vorticity at the cell center:

$$\omega'_{i,j} = \frac{(v'''_{i+1,j+1} - v'''_{i,j+1}) + (v'''_{i+1,j} - v'''_{i,j})}{2h} - \frac{(u'''_{i+1,j+1} - u'''_{i+1,j}) + (u'''_{i,j+1} - u'''_{i,j})}{2h} \quad (3.7)$$

Then take an average of ω' to get the vorticity ω'' at grid node (i, j) :

$$\omega''_{i,j} = \frac{\omega'_{i,j} + \omega'_{i-1,j} + \omega'_{i-1,j-1} + \omega'_{i,j-1}}{4} \quad (3.8)$$

Confinement Direction: Unit Vector \hat{n}

For a free vortex, the unit vector \hat{n} , which points away from the centroid of the vortical region, is computed at the grid node by

$$\hat{n} = -\frac{\nabla \eta}{|\nabla \eta|} \quad (3.9)$$

where η is a scalar which is a confinement variable. η is the magnitude of the vorticity $\vec{\omega}$. Let $\eta = |\vec{\omega}|$. We use a box scheme to get derivatives at the cell centers:

$$\omega^x_{i,j} = \frac{(\eta_{i,j} - \eta_{i-1,j}) + (\eta_{i,j-1} - \eta_{i-1,j-1})}{2h} \quad (3.10)$$

$$\omega^y_{i,j} = \frac{(\eta_{i,j} - \eta_{i,j-1}) + (\eta_{i-1,j} - \eta_{i-1,j-1})}{2h} \quad (3.11)$$

$$\nabla \eta_{i,j} = (\omega^x_{i,j}, \omega^y_{i,j})^\dagger \quad (3.12)$$

$$|\nabla \eta_{i,j}| = \sqrt{(\omega^x_{i,j})^2 + (\omega^y_{i,j})^2} \quad (3.13)$$

where $\omega^x_{i,j}$ and $\omega^y_{i,j}$ are the components of $\nabla \eta_{i,j}$ in the directions of x and y , respectively. Then the unit vector \hat{n}_ω is

$$\hat{n}_{\omega,i,j} = (n^x_{\omega,i,j}, n^y_{\omega,i,j})^\dagger \quad (3.14)$$

$$n_{\omega,i,j}^x = \frac{\omega_{i,j}^x}{|\nabla\eta_{i,j}|}$$

$$n_{\omega,i,j}^y = \frac{\omega_{i,j}^y}{|\nabla\eta_{i,j}|}$$

For the cylinder surface boundary layer, the unit vector $\hat{n}_{s,i,j}$ is

$$\hat{n}_{s,i,j} = (n_{s,i,j}^x, n_{s,i,j}^y)^\dagger \quad (3.15)$$

$$n_{s,i,j}^x = (x_{i,j} - x_c)/r_{i,j}$$

$$n_{s,i,j}^y = (y_{i,j} - y_c)/r_{i,j}$$

Then we can get the new velocity field by adding vorticity confinement. On the surface of the cylinder

$$\vec{q}_{i,j}''' = \vec{q}_{i,j}'' + \varepsilon_s \Delta t \hat{n}_{s,i,j} \times \vec{\omega}_{i,j}'' + \mu_s \Delta t \nabla^2 \vec{q}_{i,j}''' \quad (3.16)$$

Outside the cylinder, we have

$$\vec{q}_{i,j}''' = \vec{q}_{i,j}'' - \varepsilon_\omega \Delta t \hat{n}_{\omega,i,j} \times \vec{\omega}_{i,j}'' + \mu_\omega \Delta t \nabla^2 \vec{q}_{i,j}''' \quad (3.17)$$

where μ_s and μ_ω are the diffusion parameters for computing the velocity on the body surface and free vortices, respectively; ε_s and ε_ω are the confinement parameters for computing the velocity on the body surface and free vortices, respectively.

Mass Balance

A potential is solved on the Cartesian grid so that the sum of the gradients of the potential and the convected velocity with corrections enforces mass conservation.

$$\vec{q}_{i,j}^{n+1} = \vec{q}_{i,j}''' + \nabla\phi_{i,j}^{n+1} \quad (3.18)$$

where the potential $\nabla\phi^{n+1}$ satisfies the Poisson Equation

$$\nabla^2\phi^{n+1} = -\vec{\nabla} \cdot \vec{q}''' \quad (3.19)$$

3.2 Test Cases and Results

3.2.1 Case 1: Circular Flow

Initial Flow field

To demonstrate that this "bare" *Vorticity Confinement* method on Cartesian grids can work well, a 2-D irrotational circular flow field around a circular cylinder is investigated with no far field flow. For this case, the actual flow is axisymmetric and satisfies the relation

$$\begin{cases} q = 0, & r < R_c \\ q = \frac{\Gamma \hat{e}_\theta}{r}, & r \geq R_c \end{cases}$$

where R_c is the radius of the cylinder, r is the distance of a point to the center of the cylinder, Γ is a constant and \hat{e}_θ is a unit vector in the axi direction.

A square domain with the cylinder at the center is chosen. $R_c = 20$ and $R_b = 63$ is the half length of the square side in units of grid cell size. Indices c and b represent the two boundaries shown in Figure 3.3. The grid is 128×128 .

Initially, the velocity of the flow is:

$$\vec{q}_{i,j}^0 = (u_{i,j}^0, v_{i,j}^0)^\dagger \quad (3.20)$$

When $r_{i,j} \geq R_c$,

$$\begin{cases} u_{i,j}^0 &= -y_{i,j} R_c / r_{i,j}^2 \\ v_{i,j}^0 &= x_{i,j} R_c / r_{i,j}^2 \end{cases}$$

And when $r_{i,j} < R_c$,

$$u_{i,j}^0 = v_{i,j}^0 = 0$$

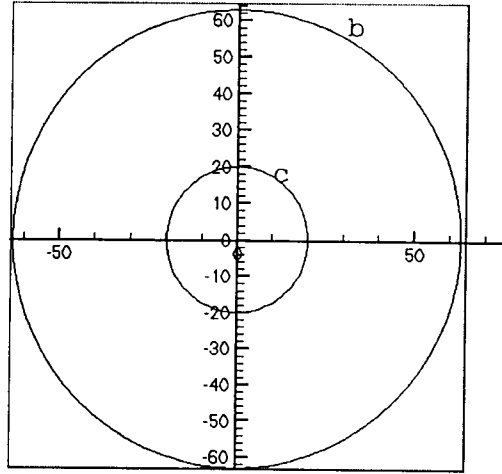


Figure 3.3: Flow Boundaries

$-64 \leq i, j \leq 64$. Figure 3.4 shows the initial velocity field.

Boundary Condition

The flow fields in the domains of $r < R_c$ and $r > R_b$ are kept constant. The velocity at the boundaries c and b is linearly extrapolated from the above domains.

Results and Discussions

$$\begin{aligned}\sigma &= -\nabla \cdot \vec{q} \\ &= -\left(\frac{\partial u}{\partial x} + \frac{\partial v}{\partial y}\right)\end{aligned}$$

is computed using a box scheme:

$$\sigma_{i,j} = -\left(\frac{u_{i+1,j+1} + u_{i+1,j} - u_{i,j} - u_{i,j+1}}{2h} + \frac{v_{i+1,j+1} + v_{i,j+1} - v_{i+1,j} - v_{i,j}}{2h}\right) \quad (3.21)$$

σ should be zero as stated before, which is the term on the right of equation (3.19);

The results show that $\sigma < 0.005$, which is very small.

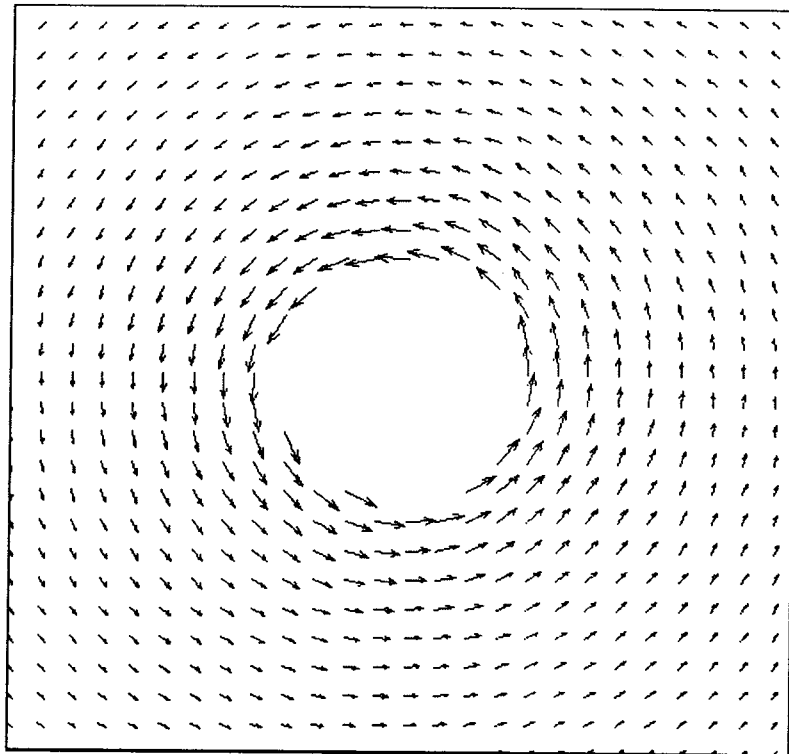


Figure 3.4: Initial Flow Velocity Field

Figure 3.5-Figure 3.7 show vorticity contours for the initial flow field, flow field after 2048 times convection with $\Delta t = 0.5$ with *Vorticity Confinement* methods, and the flow field after 2048 time steps with $\Delta t = 0.5$ without *Vorticity Confinement*, respectively. It can be seen that there is a large difference between the two cases.

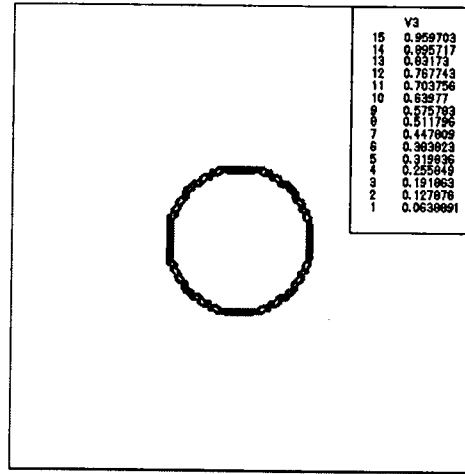


Figure 3.5: Initial Vorticity Contours, $t = 0$; $\omega_{max} = 0.9597$, $\omega_{min} = 0.0639$

Plots are made for the variables vorticity ω , radial velocity q_r , and tangential velocity q_t , where

$$q_r = \frac{\vec{q} \cdot \vec{r}}{|\vec{r}|} = \frac{xu + yv}{\sqrt{x^2 + y^2}} \quad (3.22)$$

$$q_t = \frac{\vec{q} \times \vec{r}}{|\vec{r}|} = \frac{yu - xv}{\sqrt{x^2 + y^2}} \quad (3.23)$$

For ideal convection without diffusion, q_r should be zero, which represents the velocity component in the radial direction; q_t has a maximum magnitude 1 on the surface of the cylinder, which represents the velocity component in the tangential direction; vorticity ω should remain the same as the initial flow field, with a value 0

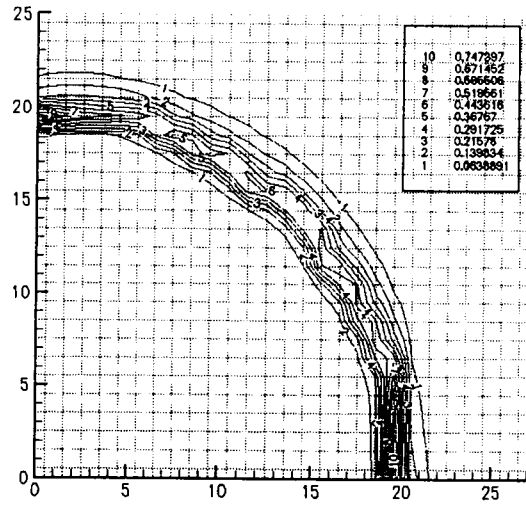


Figure 3.6: Expanded View of Vorticity Contours with *Vorticity Confinement*, $t = 1024$; $\omega_{max} = 0.7474$, $\omega_{min} = 0.0639$

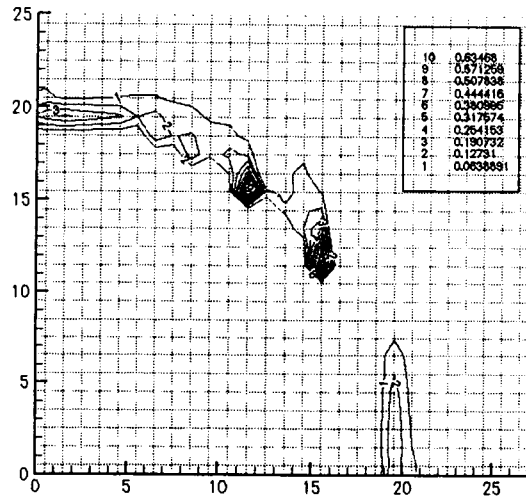


Figure 3.7: Expanded View of Vorticity Contours without *Vorticity Confinement*, $t = 1024$; $\omega_{max} = 0.6347$, $\omega_{min} = 0.0639$

in all the flow field except on the surface of the cylinder.

The plots represent the values of the variables and the corresponding r at each separate grid points. Since the initial flow is a tangential flow, the flow variables would be only a function of r and the plots should be single lines if there is no numerical error. In the plots of computation results, scatter is expected. The scatter is a measure of non-isotropic numerical effects since they should depend on the angle of the flow with respect to the grid. Isotropic effects can also, of course, be determined.

Figure 3.8 shows the initial vorticity distribution versus r . The pulse-like vorticity distribution in Figure 3.9 (with *Vorticity Confinement*) spreads over as thin as 4 cells close to $r = 20$, which is the radius of the cylinder. At the other points where $|r - 20| > 2$, ω is very small and is close enough to zero. The vortex is highly concentrated on the surface of the cylinder. While in Figure 3.10 (without *Vorticity Confinement*), ω is between 0.02 and 0.1 in a wide range of r . This is the result of numerical diffusion. Initially $q_r = 0$ everywhere because of the tangential characteristics of this flow. Figure 3.11 shows the result of *Vorticity Confinement*. At most points $|q_r| < 0.01$. Only at a few points close to $r = 20$, which are on the cylinder surface, is the velocity component in the radial direction increased. Figure 3.12 shows the result without *Vorticity Confinement*. The difference is obvious. $|q_r| > 0.01$ at a large number of points. The flow field is deformed badly. Again, Figure 3.14 shows a similar pattern for the $q_t - r$ plot to that of the theoretical flow field as in Figure 3.13 with $q_{tmax} > 0.8$. While Figure 3.15 shows a very different pattern with $q_{tmax} = 0.4$. From the above results, we can see that the *Vorticity Confinement* method can preserve the vorticity in a very thin region around the body surface, with only a regular Cartesian grid.

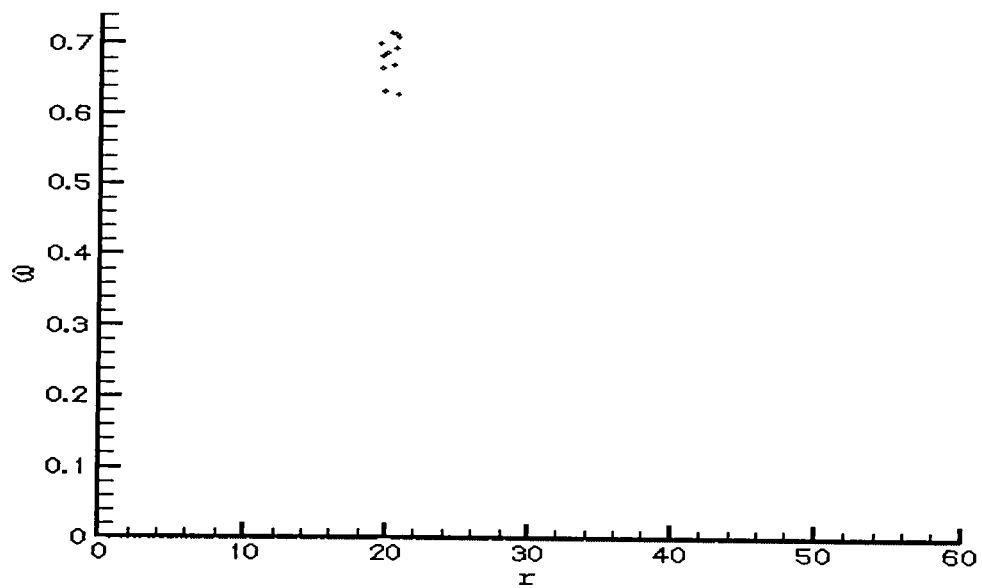


Figure 3.8: Initial Vorticity-radius

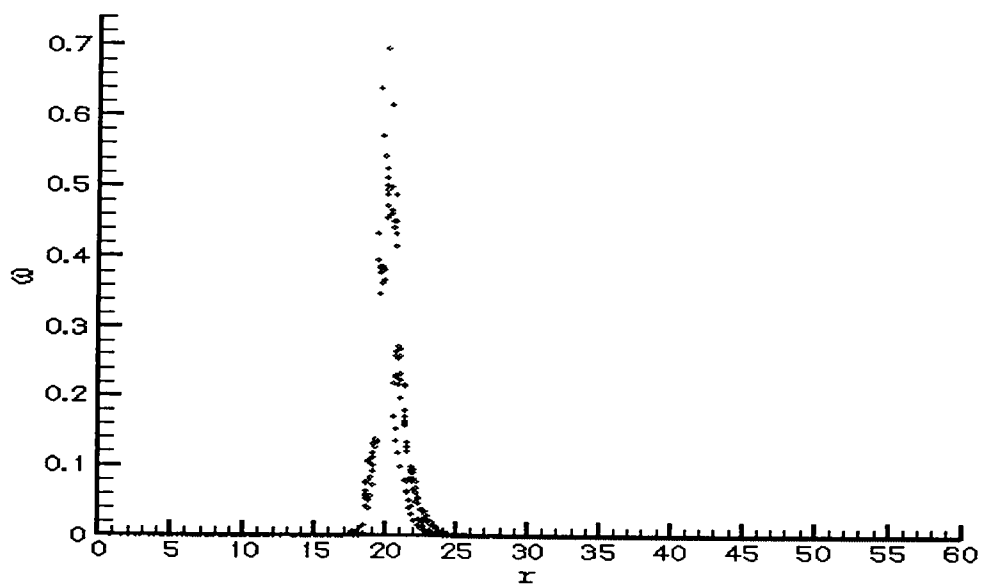


Figure 3.9: $\omega - r$ with *Vorticity Confinement*, $t = 1024$

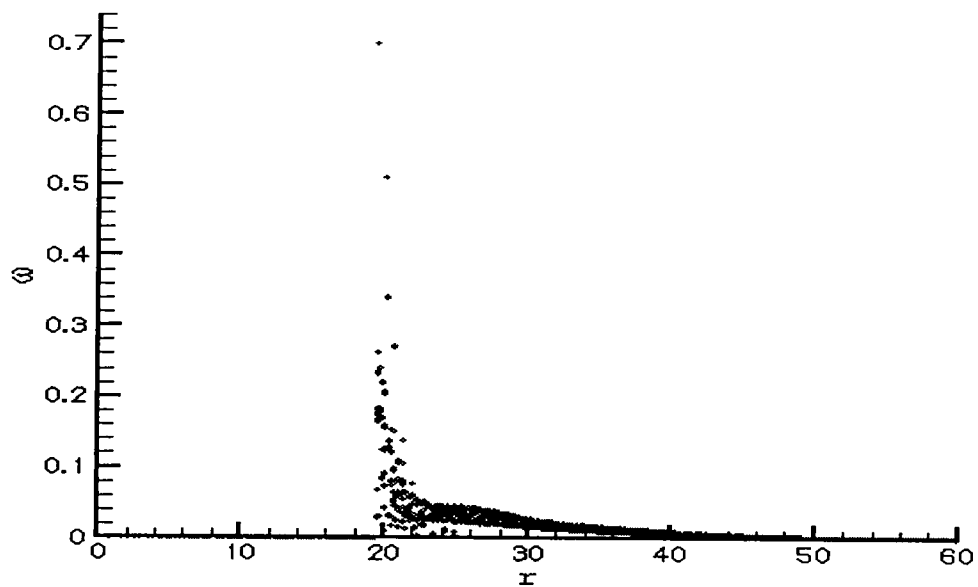


Figure 3.10: $\omega - r$ without *Vorticity Confinement*, $t = 1024$

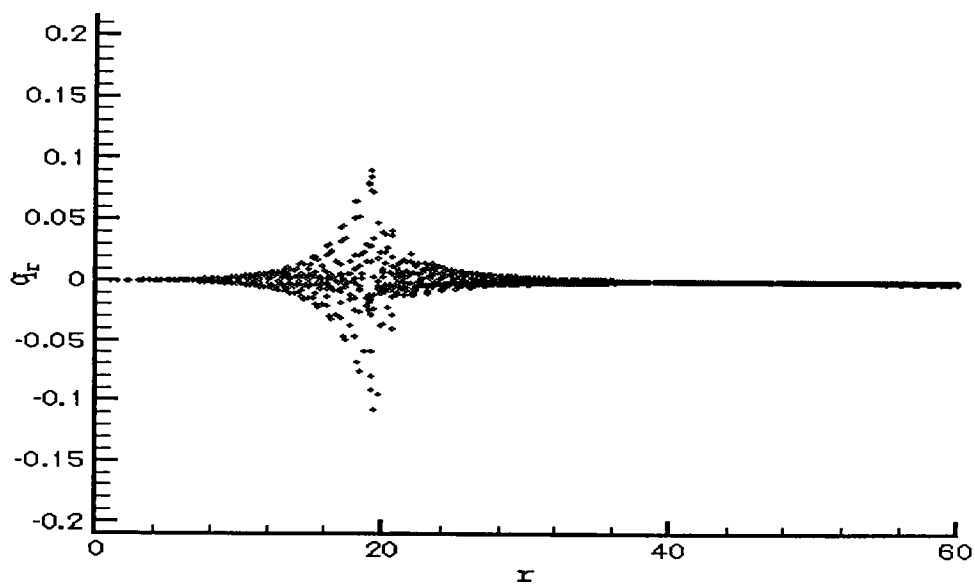


Figure 3.11: $q_r - r$ with *Vorticity Confinement*, $t = 1024$

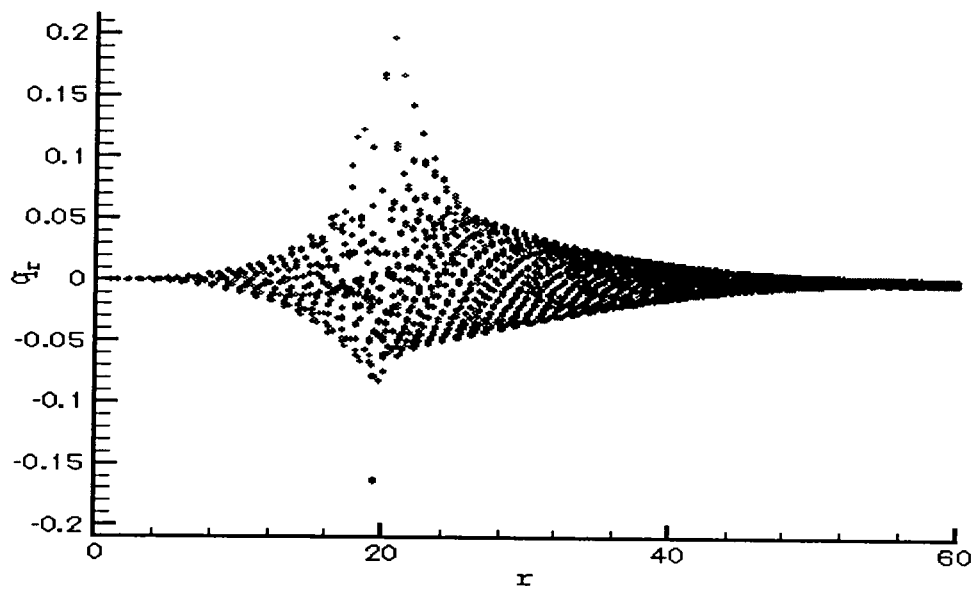


Figure 3.12: $q_r - r$ without *Vorticity Confinement*, $t = 1024$

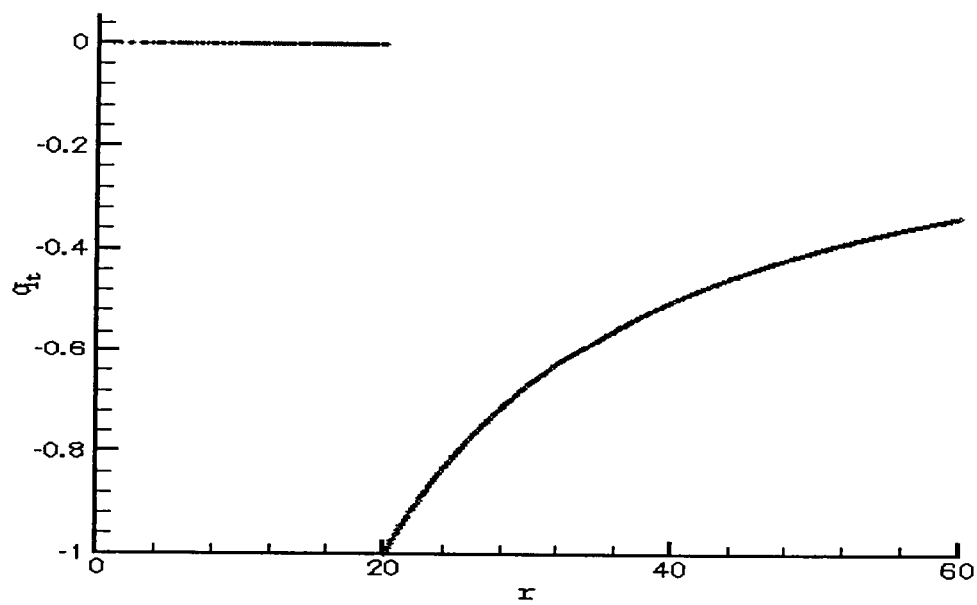


Figure 3.13: Initial $q_t - r$

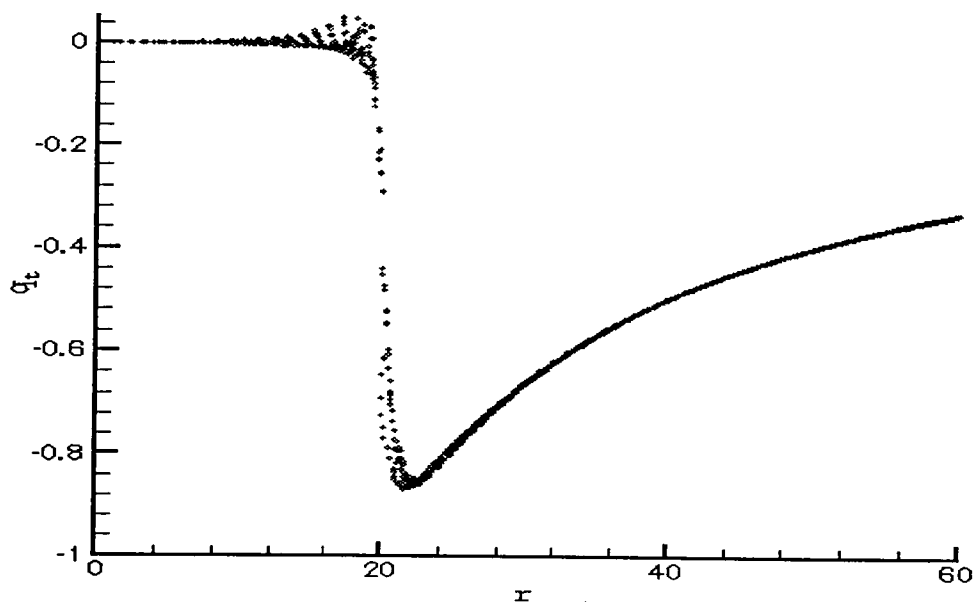


Figure 3.14: $q_t - r$ with *Vorticity Confinement*, $t = 1024$

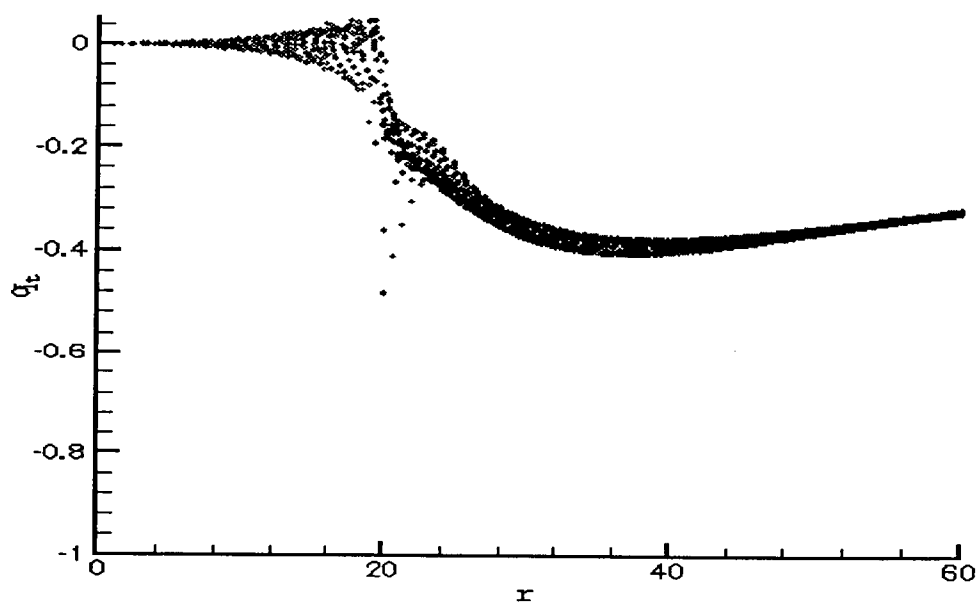


Figure 3.15: $q_t - r$ without *Vorticity Confinement*, $t = 1024$

3.2.2 Case 2: Uniform Far Field Flow

A 2-D uniform incoming flow passing around a circular cylinder is investigated.

We want to develop a method using only uniform Cartesian grids for complex geometrics which may have variations in local radius of curvature. And we need to know how to model layer effects. Since a general 3-D high Reynolds number flow over a complex body will depend on the various components, if we are to attempt to use uniform Cartesian grids we must know the characteristics of the shed vorticity over the various parts. For this reason, we study circular cylinders with various ratios of radius to grid size. We apply this simple "bare" *Vorticity Confinement* method on 2-D cylinders with a range of radii in terms of grid cell size to try to get reasonable approximations for the separation and to capture and maintain the shed vortices.

Since a general 3-D high Reynolds number flow over a complex body will depend on the various components, if we are to attempt to use uniform Cartesian grids we must know the characteristics of the shed vorticity over the various parts. For this reason, we study circular cylinders with various ratios of radius to grid size.

For our study, the vortex separation and free wake pattern are the focused issues.

Background: Eddy Shedding and Strouhal Number

When a fluid flows past a circular cylinder, regions of disturbed flow are always formed around it. For different Reynolds numbers (Re), the flow field may be in a state of laminar, transition or turbulence[1][2].

When Re is small, the wake behind cylinder is stable and the eddies remain attached to the body. When Re is about 40, the wake behind the cylinder becomes

unstable. Oscillations in the wake grow in amplitude and finally roll up into discrete vortices with a very regular spacing. This trail of vortices in the wake is known as the *Karman Vortex street*. The vortices travel downstream at a speed slightly less than the free stream velocity, U_∞ . They are not turbulent, and the flow near the cylinder remains steady with two attached eddies. The frequency of this oscillation, f , when non-dimensionalized by the diameter d and velocity U_∞ , is called the Strouhal number. It is defined as

$$St = \frac{fD}{U_\infty} \quad (3.24)$$

The Strouhal number varies slightly with Re but is roughly 0.2 over a wide range in Re . As the Reynolds number increases, the vortex street forms closer to the cylinder, until finally the attached eddies themselves begin to oscillate. When Re is between 60 and 100, the attached eddies begin to give way to eddies that alternately form and then shed. We now have an unsteady flow near the cylinder, the drag force oscillates with the formation of each eddy, and the top-to-bottom asymmetry of the flow gives rise to an oscillating lift force. At a Reynolds number of 200, the vortex street becomes unstable to bends in the spanwise direction. As one goes further downstream these bends grow and the wake ultimately becomes turbulent. In the range of $200 < Re < 400$, the Strouhal number loses its regular, well-defined character. When $Re > 400$, the vortices themselves become turbulent. The turbulence within the vortices gives them a different velocity profile and restores the spanwise coherence. This restabilizes the Strouhal number and it returns to its value of 0.2. When $Re < 3 \times 10^5$, laminar boundary layer separates at 80° . When $3 \times 10^5 < Re < 3 \times 10^6$, separated region becomes turbulent, reattaches, and separates again at 120° . When $Re > 3 \times 10^6$,

turbulent boundary layer begins on front and separates on back. Over the high Reynolds number range, a time history of the velocity at any point has a large spectral component at the Strouhal frequency of 0.2. See Figure 3.16 and Figure 3.17.

So, there are two different modes of eddy shedding[1]:

1. Low-speed mode. The eddy street starts as the trail instability. The eddies are formed by the roll-up of free shear layers at crests and troughs along the trail. The eddies grow along the wake while carried downstream and St increases with rising Re .
2. High-speed mode. The eddies are formed behind the cylinder by the roll-up of free shear layers in an almost fixed location. The eddy street starts by the alternate shedding of fully grown eddies. The eddies diffuse and decay along the wake while carried downstream and St is almost constant with rising Re .

Initial Flow Field

Initially, the flow field is set to a uniform flow by assuming that the free stream is in the x direction in this 2-D Cartesian system. The velocity, $\vec{q} = (u, v)^T$, at time $t = 0$ is set to:

$$\vec{q}^0 = (U_\infty, 0)^T \quad (3.25)$$

which numerically is, for each grid node (i, j) in the computation domain,

$$\begin{cases} u_{i,j}^0 &= U_\infty = 1 \\ v_{i,j}^0 &= 0 \end{cases}$$

For all the following computations,

$$\Delta t = 0.5$$

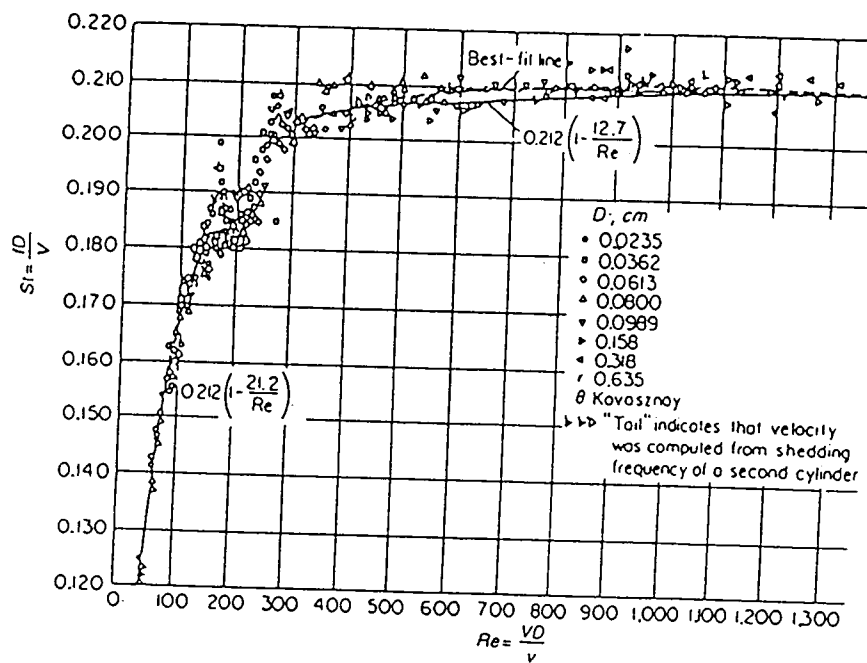


Figure 3.16: Variation of St in terms of Re , Roshko(1954P)

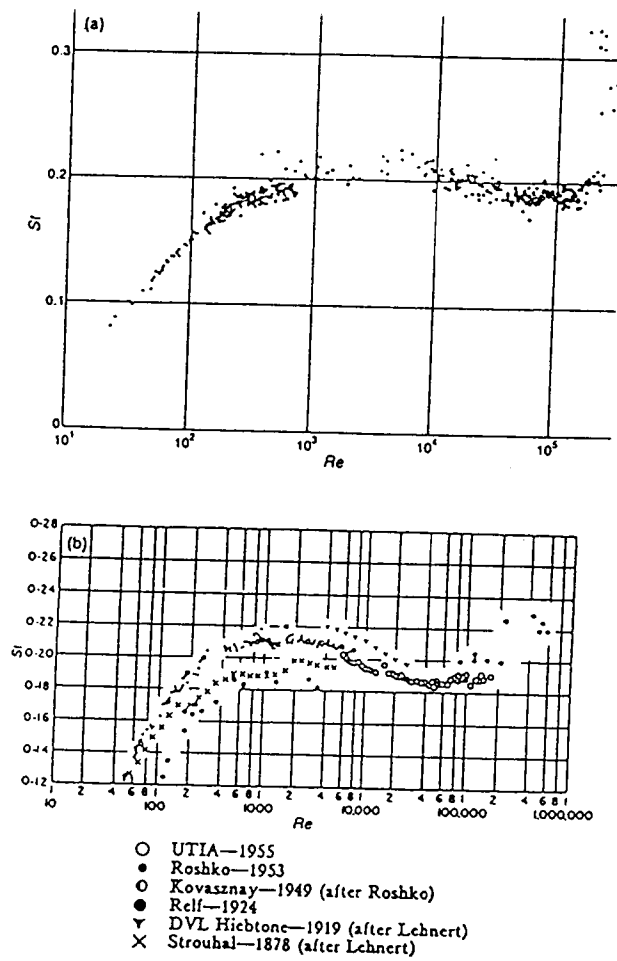


Figure 3.17: Compilation of St versus Re : (a) Drescher(1956J) ○ French data, □ Tyler, ◇ DVL data, ○ AVA($Re > 1k$) (b) Etkin *et al.* (1957J)

$$\Delta x = \Delta y = h = 1$$

but different grids and cylinder sizes may be used.

Results	Grids	R_c in terms of grid cells
1	320×128	10
2	320×128	10
3	640×128	10
4	160×64	5
5	80×32	2.5

Boundary Conditions

For all the following computations, the far field boundary condition is explicitly imposed during velocity convection and corrections, at every time step. At the upstream boundary, the velocity is set to the free stream velocity. And the velocity at the other boundaries of the computation domain are linearly extrapolated from the inner domain.

Result 1

First, the results using *Vorticity Confinement* method are presented. The size of the cylinder and the grid are stated above. Figure 3.18 shows the initial velocity field. Figure 3.19 shows the velocity field at $t = 1024$. $\varepsilon_\omega = 0.04$, $\varepsilon_s = 0.1$, $\mu_s = \mu_\omega = 0.05$ are chosen for this case. We can see the oscillation of the wake.

Figure 3.20 and Figure 3.21 show the vorticity contours at $t = 992$ and $t = 1024$, respectively. Figure 3.22 is an expanded view of the vorticity contour plot for part of the surface boundary at $t = 1024$. We can see that the vortical region around cylinder is confined as thin as $2 \sim 3$ cells.

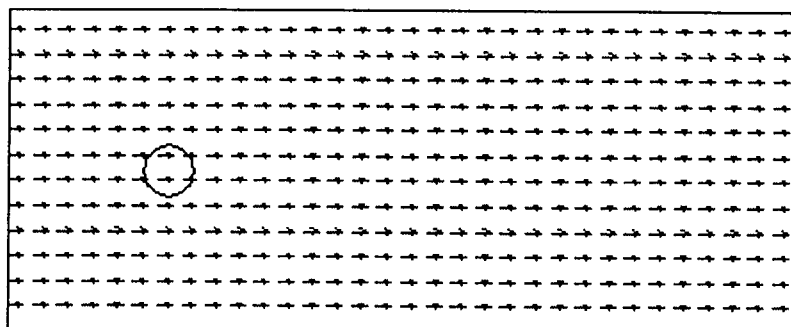


Figure 3.18: Initial Velocity Field

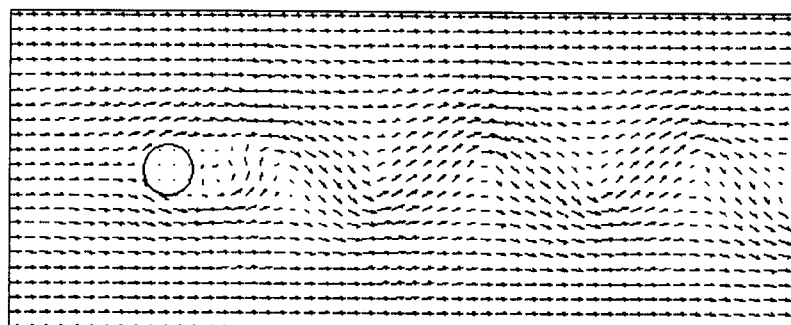


Figure 3.19: Velocity Field; $t = 1024$

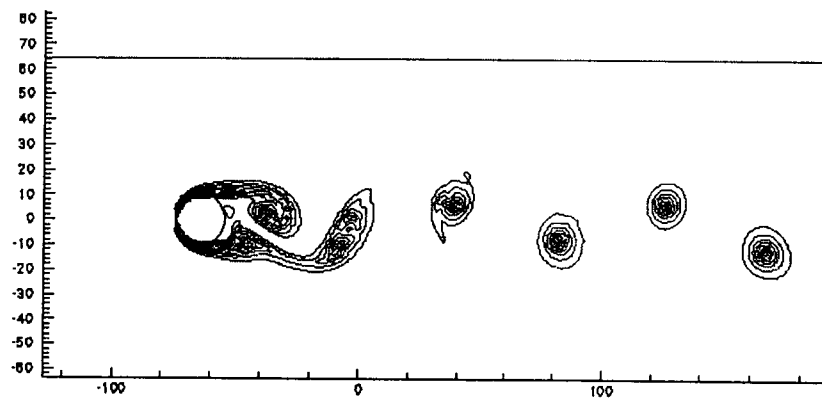


Figure 3.20: Vorticity Contours; $R_c = 10$; $t = 992$



Figure 3.21: Vorticity Contours; $R_c = 10$; $t = 1024$

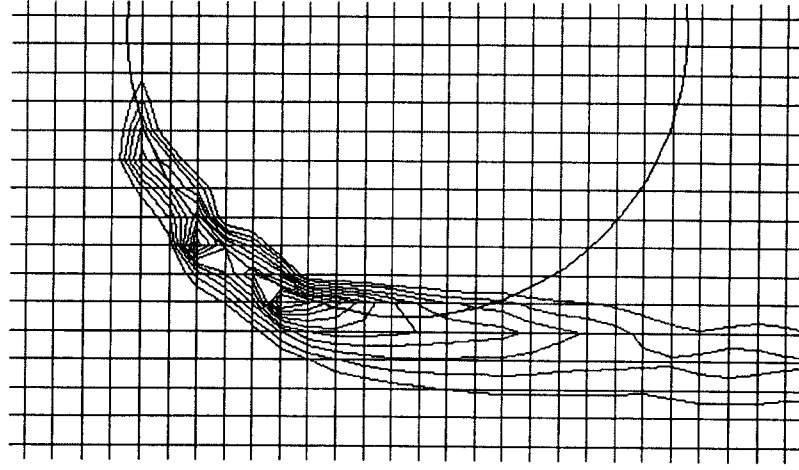


Figure 3.22: Expanded View of Vorticity Contours; $R_c = 10$; $t = 1024$; $\omega_{max} = 1.063$, $\omega_{min} = 0.2$

Figure 3.23 and Figure 3.24 are other expanded views for the vorticity contour plots, at $t = 992$ and $t = 1024$, respectively. From the definition of Strouhal number, we can get

$$St_v = \frac{fD}{U_\infty} = \frac{D}{t_v U_\infty} = \frac{2R_c}{(t_v u_v)(\frac{U_\infty}{u_v})} = \frac{2R_c}{x_v} \frac{u_v}{U_\infty} \quad (3.26)$$

where St_v is the Strouhal number computed from the vortices in the free wake of the results. f is vortex shedding frequency, and

$$t_v = \frac{1}{f}$$

is the time interval between two shed neighbour vortices on the same side, such as 1 and 3 in Figure 3.23 and Figure 3.24. And

$$x_v = t_v u_v$$

is the spacing between the two vortices along x direction. Compare the position of

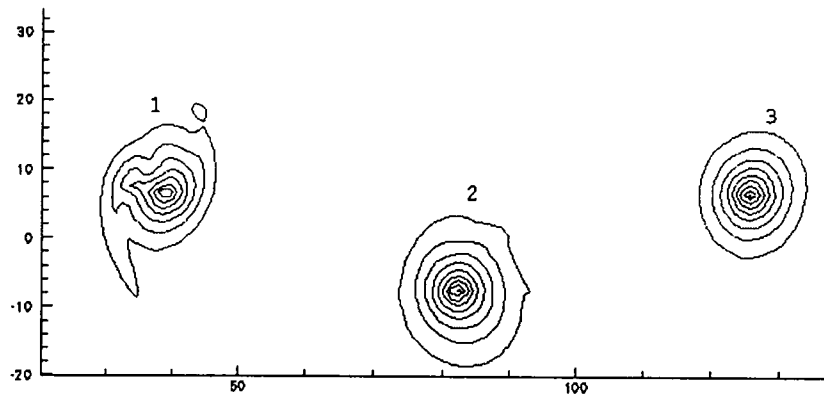


Figure 3.23: Expanded View of the Vorticity Contours; $R_c = 10$; $t = 992$

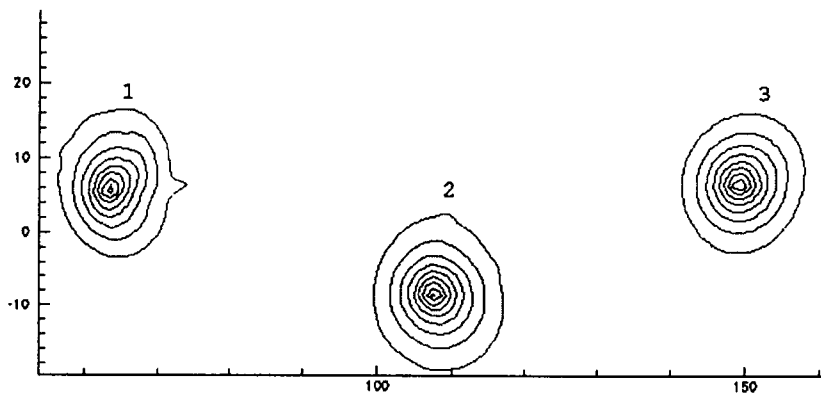


Figure 3.24: Expanded View of the Vorticity Contours; $R_c = 10$; $t = 1024$

vortex 2 in Figure 3.23 and Figure 3.24, we get

$$x_{v2} = 108 - 81 = 27$$

the time difference between the two figures is

$$t_v = 1024 - 992 = 32$$

Index $v2$ indicates vortex 2. Then

$$u_v = \frac{x_{v2}}{t_v} = \frac{27}{32} = 0.84$$

$$St_v = \frac{2 \times 10}{84} \frac{0.84}{1} = 0.20$$

which is close to the the experimental values reviewed in the background section.

Result 2

In order to simulate a physical spreading of a vortex (due to viscosity or turbulence), and to demonstrate that not only this simple "bare" method but also much more sophisticated models can be easily implemented, a simple varication of *varepsilon* was taken which deviated from the constant value that used in Result 1. ε_ω was reduced linearly in x direction from $\varepsilon_\omega = 0.04$ behind the cylinder to $\varepsilon_\omega = 0$ at the right end of the domain. Figure 3.25 shows the result of $t = 1024$. The effects of diffusion at downstream of the cylinder are obvious.

Comparing Figure 3.21 and Figure 3.25, we can that see the corresponding vortices are essentially at the same positions although those in Figure 3.25 are much bigger than those in Figure 3.21. This implies that *Vorticity Confinement* doesn't significantly change the momentum of the flow.

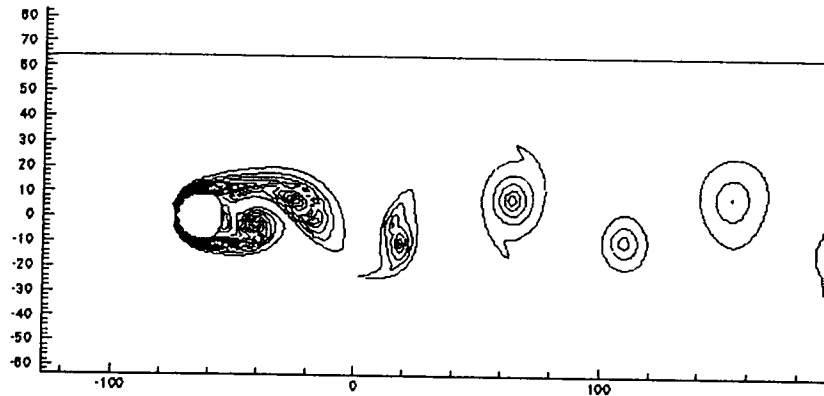


Figure 3.25: Vorticity Contours with Reduced ε_ω ; $R_c = 10$; $t = 1024$

Result 3

This case was computed to demonstrate that there are no significant numerical effects even when the vortices are convected over long distances. Since the paper size is limited, we can only show Fig 3.26 as an example.

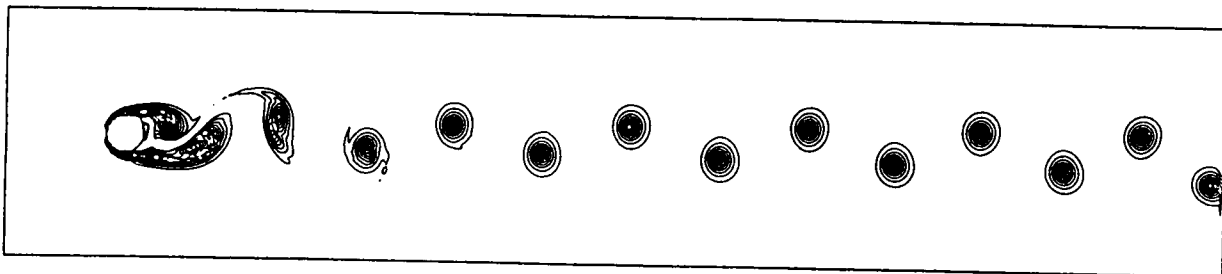


Figure 3.26: Vorticity Contours; $R_c = 10$; Grids : 640×128 ; $t = 2048$

Result 4

A coarser grid like 160×64 is used in this case, and the cylinder radius is $R_c = 5$ cells accordingly. $\varepsilon_\omega = 0.1, \varepsilon_s = 0.2, \mu_s = \mu_\omega = 0.001$ are chosen for this computa-

Figure 3.27 and Figure 3.28 show the vorticity contours at $t = 1008$ and $t = 1024$, respectively. Figure 3.29 and Figure 3.30 are the expanded views of Figure 3.27 and Figure 3.28, respectively.

$$\begin{aligned} u_v &= \frac{40 - 26}{1024 - 1008} \\ &= 0.81 \end{aligned}$$

$$\begin{aligned} St_v &= \frac{2 \cdot R_c}{x_v} \frac{u_v}{U_\infty} \\ &= \frac{2 \times 5}{61 - 19} \frac{0.81}{1} \\ &= 0.19 \end{aligned}$$

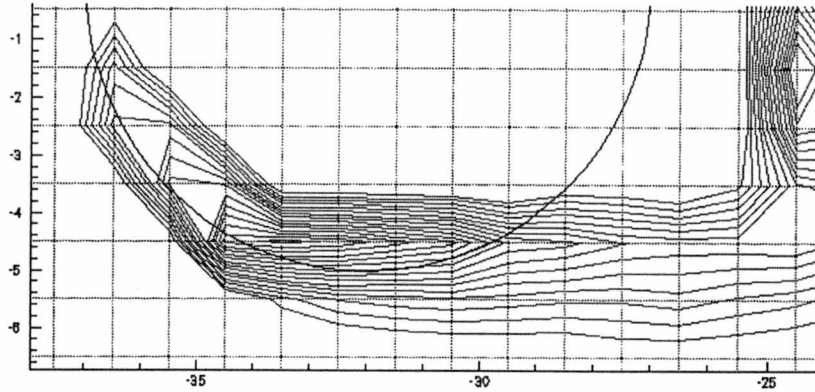


Figure 3.27: Expanded View of Vorticity Contours; $R_c = 5$; $t = 1024$; $\omega_{max} = 1.026$, $\omega_{min} = 0.2$

Figure 3.31 shows an expanded view of vorticity contours near the cylinder surface at $t = 1024$. Most vorticity is confined to 2 cells.



Figure 3.28: Vorticity Contours; $R_c = 5$; $t = 1008$

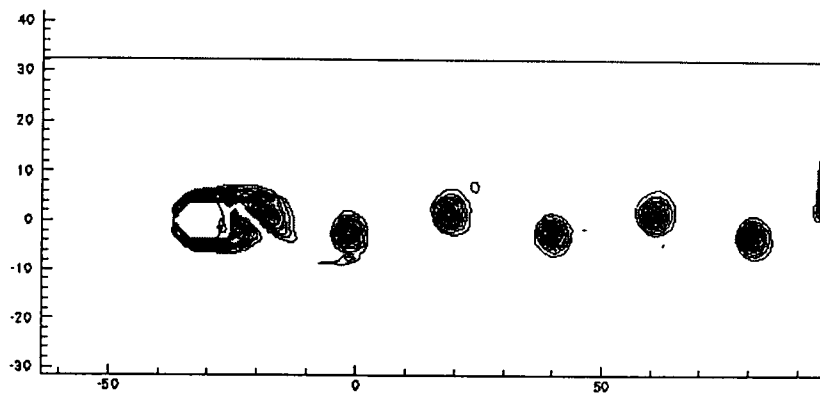


Figure 3.29: Vorticity Contours; $R_c = 5$; $t = 1024$

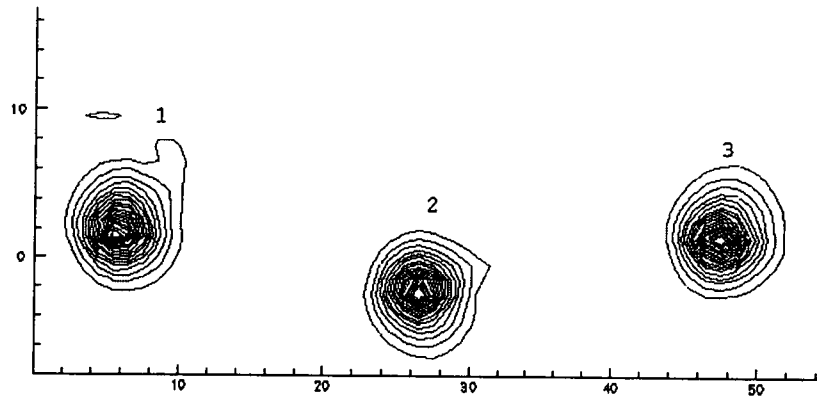


Figure 3.30: Expanded View of Vorticity Contours; $R_c = 5$; $t = 1008$

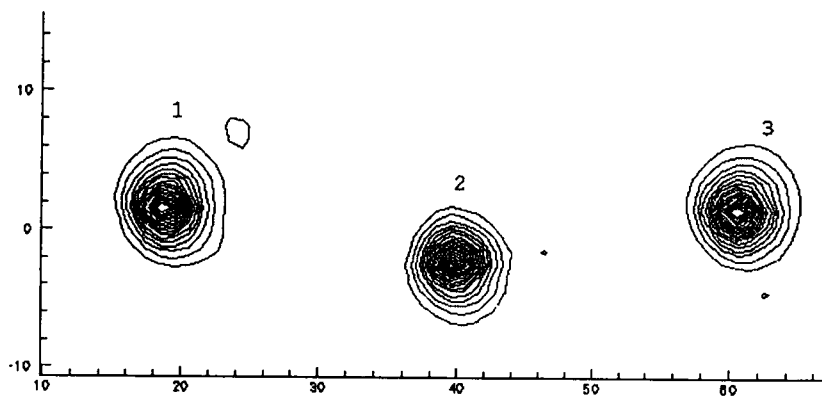


Figure 3.31: Expanded View of Vorticity Contours; $R_c = 5$; $t = 1024$

Result 5

In this case, the grid is 80×32 , and the cylinder radius is $R_c = 2.5$ cells. $\varepsilon_\omega = 0.17, \varepsilon_s = 0.3, \mu_s = \mu_\omega = 0.05$ are chosen for computing. Figure 3.32 and Figure 3.33 show the vorticity contours at $t = 1016$ and $t = 1024$, respectively. Figure 3.34 and Figure 3.35 are the expanded views of Figure 3.32 and Figure 3.33, respectively.

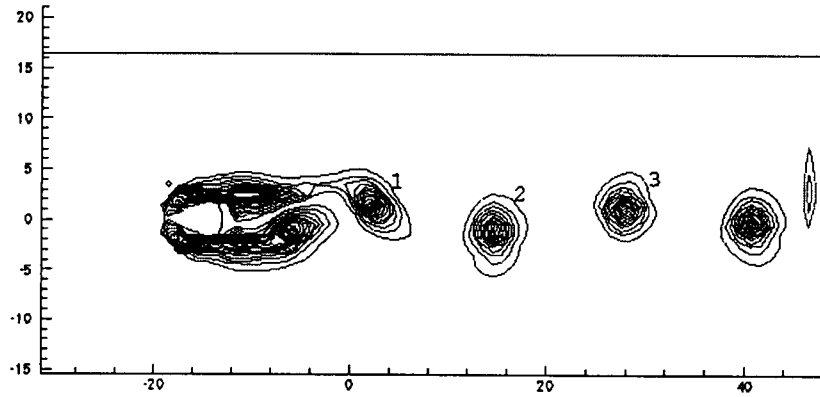


Figure 3.32: Vorticity Contours; $R_c = 2.5$; $t = 1016$

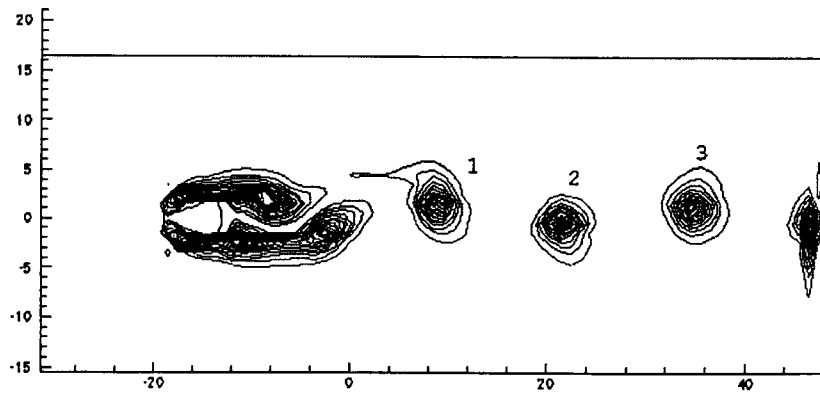


Figure 3.33: Vorticity Contours; $R_c = 2.5$; $t = 1024$

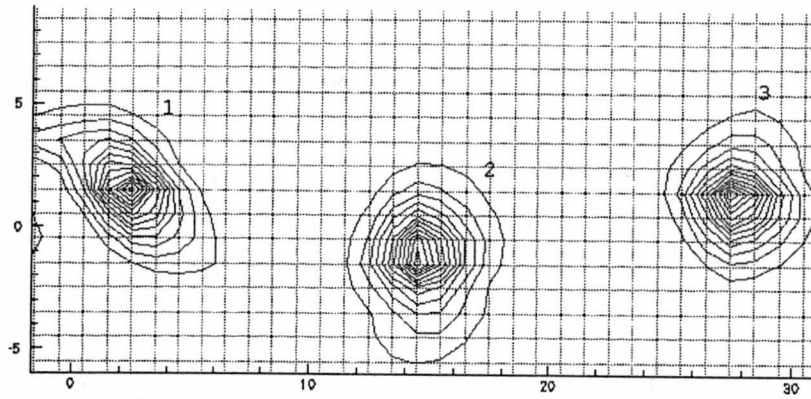


Figure 3.34: Expanded View of Vorticity Contours; $R_c = 2.5$; $t = 1016$

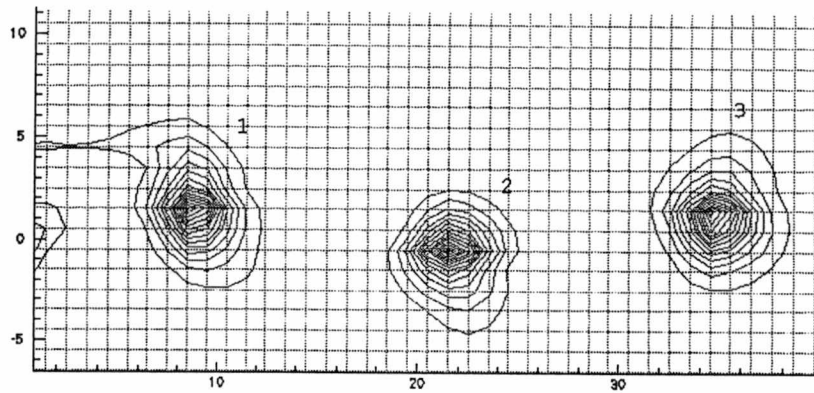


Figure 3.35: Expanded View of Vorticity Contours; $R_c = 2.5$; $t = 1024$

$$\begin{aligned}
 u_v &= \frac{22 - 15}{1024 - 1016} \\
 &= 0.625
 \end{aligned}$$

$$\begin{aligned}
 St_v &= \frac{2 \cdot R_c}{x_v} \frac{u_v}{U_\infty} \\
 &= \frac{2 \times 3}{35 - 9} \frac{0.875}{1} \\
 &= 0.17
 \end{aligned}$$

The parameters ε and μ could be chosen in a certain range. What I used is only one set of those which can lead to a steady state solution. More details will be investigated in the future.

Figure 3.36 shows the expanded view of vorticity contours near the cylinder surface. Most vorticity is confined to 2 cells.

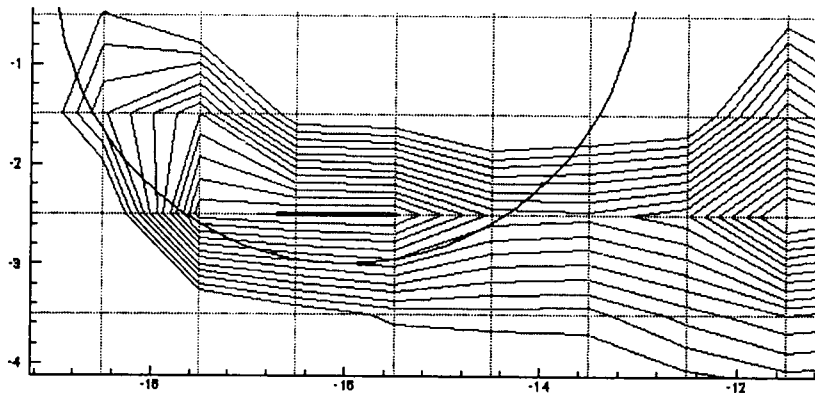


Figure 3.36: Expanded View of Vorticity Contours; $R_c = 2.5$; $t = 1024$; $\omega_{max} = 1.104$, $\omega_{min} = 0.2$

Discussion

From the above results, we can see that

1. vortices are generated periodically from the cylinder surface.
2. secondary separation on the cylinder surface can be seen even using relatively coarse grids such as in Result 1 to Result 4. Only when the grid is too coarse, for example, when the expected secondary separation region is smaller than a grid cell (as in Result 5), can it not be seen.
3. the vortices are generated up-and-down alternatively to form a flow pattern similar to a *Von Karman Vortex Street* which is the steady state of a 2-D flow around a circular cylinder.
4. the ratio of vertical to horizontal spacing is about 30% smaller than in *Von Karman's* theoretical model. This feature may be affected by the exact confinement model used and will be studied in the future.
5. the shed vortices are about the same size as the cylinder.
6. even when the grid is as coarse as that in Result 5, the vorticity around the surface boundary can be confined to as thin as $2 \sim 3$ cells.
7. the vortex shedding frequency (Strouhal number) is close to that seen experimentally over a large range of Reynolds numbers.
8. the vertical separation or spreading of the vortex street as it moves downstream remains close to the cylinder diameter for all three cylinders studied, for the simple "bare" confinement method studied.

9. as explained in point 4, the shape of the wake will be changed to simulate different turbulent regimes at different (high) Reynolds numbers by the addition of other modeling terms using the current "bare" method as a base. The main objective of the current study was to develop a method to very efficiently compute flows on uniform Cartesian grids that approximates physical high Reynolds number cases.

Chapter 4

Conclusion

The *Vorticity Confinement* method was introduced. The method treats vortical layers as controlled solitary-wave-like objects. Applications of the simple "bare" scheme to flows around circular cylinder have been presented to demonstrate the following features of this numerical approach:

1. It only involves simple, coarse uniform Cartesian grids. No body-conforming grid is needed.
2. It yields reasonable results even using a very coarse grid such as for a cylinder with a radius of 2.5 grid cells.
3. The method does not involve second order viscous diffusion terms in partial differential equations, which are typically used in the boundary layers to try to model the turbulence effects in a Reynolds averaged way. Since the boundary layers are thin, discretizing these model terms in very thin grid cells and body-conforming grids usually leads to computational difficulties.
4. The method treats boundary layers using a pair of terms which result in stable structures spread over only $2 \sim 3$ cells. This method directly controls the

structure on the grid in a very efficient way.

5. The simplest "bare" form of this method, without any turbulence modeling terms, results in reasonable simulations of vorticity generation, separation and convection.
6. The method provides a basic way to add additional modeling terms while keeping the computational efficiency so that details of turbulent flows at different Reynolds numbers can be simulated (this will be studied in the future).
7. Of course without any turbulence models, we cannot get exact surface pressures, vortex separating angles, spacing of the vortices or turbulent fluctuations. But with this "bare" scheme in a coarse Cartesian grid, we can get an approximation of the whole picture of the flow field efficiently. It should be a good starting point to develop new turbulence models in order to get more detailed and accurate results.

Bibliography

Bibliography

- [1] Ronald L. Panton, *Incompressible Flow*. A Wiley-Interscience Publication.
- [2] M. M. Zdravkovich, *Flow Around Circular Cylinders*. Oxford Science Publications.
- [3] J. Steinhoff, E. Puskas, S. Babu, Y. Wenren, D. Underhill, *Computation of Thin Reatures Over Long Distances Using Solitary Waves*, AIAA paper, 1997.
- [4] J. Steinhoff, Thomas Mersch, David Underhill, Yonghu Wenren, Clin Wang, *Computational Vorticity Confinement: A Non-diffusive Eulerian Method For Vortex-dominated Flows*, UTSI preprint, 1992.
- [5] Yonghu Wenren, *A New Numerical Method for Computing Flow Over Complex Aerodynamic Configurations and Its Application to Rotor/Body Computation Using Cartesian Grids*, PhD theis, UTK, 1997.
- [6] P. Koumoutsakos, A. Leonard, *Direct Numerical Simulations Using Vortex Methods*, AIAA paper, 1989.
- [7] C. H. K. Williamson *Vortex Dynamics in the Cylinder Wake*, *Ann. Rev. Fluid. Mech.*, 1996, 28:477-539.

- [8] C. Mavriplis, L.-C. Hsu, *A Two-Dimensional Adaptive Spectral Element Method*, AIAA paper, 1997.
- [9] H. Yamada, H. Yamabe, A. Itoh, H. Hayashi *Numerical Analysis of a Flowfield Produced by a Pair of Rectilinear Vortices Approaching a Circular Cylinder*, *Fluid Dynamics Research* 3 (1988) 105-110.
- [10] C. Barbi, D. P. Favier, C. A. Maresca, *Vortex Shedding and Lock-on of a Circular Cylinder in Oscillatory Flow*, *J. Fluid Mech.* (1986) vol. 170, pp. 527-544.
- [11] A. Roshko, Experiments on the flow past a circular cylinder at very high Reynolds numbers. *Journal Fluid Mechanics*, 10, 345-56, 1961J.
- [12] M. S. Uberoi, P. Freymuth, Spectra of turbulence in wakdes behind circular cylinders. *Physics Fluids*, 12, 1359-63, (1969J)
- [13] B. J. Cantwell, An experimental study of turbulent near-wake of a circular cylinder at $Re = 140,000$. PhD thesis, Caltec, Calif, 1976P.
- [14] C. Graham, A survey of correlation length measurements of the vortex shedding process behind a circular cylinder. *Massachusetts Institute of Technology*. MIT TR 76028, 1966.
- [15] N. Kamiya, S. Suzuki, T. Nishi, On the aerodynamic force acting on a circular cylinder in the critical range of the Reynolds number. AIAA meeting, paper 79-1975, 1979.

- [16] H. Loiseau, E. Szechenyi, Dynamic lift on a cylinder in high Reynolds number flow. *Flow Induced Structural Vibrations*, E.Naudascher, ed. Springer, berlin, 755-61, 1974.
- [17] G. W. Jones, J. Cincotta, W. Walker, Aerodynamic forces on a stationay and oscillating circular cylinder at high Reynolds numbers. *NASA TR R-300*, 1-62, 1969.
- [18] L. V. Schmidt, Fluctuating force measurements upon a circular cylinder at Re up to 5×10^6 , *NASA TMX 57*, 779, 1966.

Vita

Lifan Yu was born in Shenyang, a lovely but heavily polluted and populated city, People's Republic of China. In Beijing University of Aeronautics and Astronautics, she got her Bachelor's degree in Aeroengine Design in 1993 and Master's degree in Aerospace Engineering in 1996. She entered University of Tennessee Space Institute, Tullahoma, TN, in August 1996, majoring in Mechanical Engineering.